MECHANICAL BEHAVIOUR OF ADDITIVELY MANUFACTURED LUNAR REGOLITH SIMULANT COMPONENTS

Athanasios Goulas[a], Jon G.P. Binner[b], Daniel S. Engstrøm[a], Russell A. Harris[c], Ross J. Friel[d]

[a] *Wolfson School of Mechanical, Electrical & Manufacturing Engineering, Loughborough University, Loughborough, Leicestershire, LE11 3QZ, United Kingdom*

[b] *College of Engineering and Physical Sciences, University of Birmingham, Edgbaston, Birmingham, B15 2TT, United Kingdom*

[c] *Mechanical Engineering, University of Leeds, Leeds, LS2 9JT, United Kingdom*

[d] *MAX IV Laboratory, Lund University, P.O. Box 118, SE-221 00, Lund, Sweden*

ABSTRACT

Additive manufacturing and its related techniques have frequently been put forward as a promising candidate for planetary *in-situ* manufacturing, from building life-sustaining habitats on the Moon to fabricating various replacements parts, aiming to support future extra-terrestrial human activity. This paper investigates the mechanical behaviour of lunar regolith simulant material components, which is a potential future space engineering material, manufactured by a laser-based powder bed fusion additive manufacturing system.

The influence of laser energy input during processing was associated with the evolution of component porosity, measured via optical and scanning electron microscopy in combination with gas expansion pycnometry. The compressive strength performance and Vickers micro-hardness of the components were analysed and related back to the processing history and resultant microstructure of the lunar regolith simulant build material.

Fabricated structures exhibited a relative porosity of 44 – 49% and densities ranging from 1.76 – 2.3 g cm^{-3}, with a maximum compressive strength of 4.2 ± 0.1 MPa and elastic modulus of 287.3 ± 6.6 MPa, the former is comparable to a typical masonry clay brick (3.5 MPa). The

AM parts also had an average hardness value of 657 ± 14 $HV_{0.05/15}$, better than borosilicate glass (580 HV).

This study has shed significant insight into realizing the potential of a laser-based powder bed fusion AM process to deliver functional engineering assets via *in-situ* and abundant material sources that can be potentially used for future engineering applications in aerospace and astronautics.

1 Introduction

The concept of *In-Situ* Resource Utilisation (ISRU) has been put forward since humans first set foot on the surface of the Moon. The goal of ISRU is to exploit the readily available extra-terrestrial natural resources (e.g. lunar regolith), with the long-term vision being for equipment to be sent off-world to allow the manufacture of complete outposts that will be able to host future manned missions. These will be able to sustain long duration exploratory expeditions into deep space and nearby planetary destinations [1]. Although significant time and research have been devoted to this goal, there has been minimal progress in terms of technological advancement, apart from several proof-of-concept demonstrations and feasibility studies in laboratory environments and so the work is still at a relatively low Technology Readiness Level (TRL) [2].

Additive Manufacturing (AM) – also known as 3D printing – and its related technologies, have been discussed and proposed as a highly promising solution for serving the ISRU goal of building physical assets off-world [3–7] by using the abundant and readily available natural resources onsite [8,9]. The ultimate plan is for it to operate in an autonomous manner [7], without human presence or intervention being required.

Powder Bed Fusion (PBF) is one of the 7 main process categories in the AM family; the category uses powder materials (metals, polymers and ceramics) as feedstock. Recent work has established that PBF can successfully process naturally occurring terrestrial multi-component ceramic materials of igneous origin, which act to simulate a range of key properties such as bulk chemistry, mineralogy and mechanical performance for indigenous materials found on the Moon and Mars [10–13].

Previous studies related to the concept of 3D printing using extra-terrestrial/astro-materials as feedstock, and their state-of-the art available simulants [14–16], have covered fundamental topics ranging from raw materials' physical properties [17–23] and their engineering characteristics [24–28] to the development of process parameters [11,13] for the relevant 3D printing technique. Despite all the work that has been done on the research of the materials and manufacturing mechanisms, there is still little information available on the actual mechanical performance of the fabricated components, especially in terms of relating the resulting material microstructure to the processing characteristics and method.

The work discussed in this paper consists of a study focused on investigating the laser-based additive manufacture of JSC-1A lunar mare regolith simulant components and the impact of the resulting microstructural characteristics on the mechanical behaviour of the components under standardised compression and Vickers micro-hardness testing. Such materials engineering research will aid in identifying the true potential of PBF AM-processing for delivering functional engineering assets via ISRU in the context of surface planetary manufacturing.

2 Experimental Details

2.1 Materials

This study was conducted using the JSC-1A Lunar mare regolith simulant, **Figure 1**, developed and sold by Orbitec (Orbital Technologies Corporation, Colorado, USA) in coordination with NASA's Johnson Space Centre. This simulant is a replica of the original JSC-1 lunar mare regolith simulant developed by NASA's Marshall Space Flight Centre [29] and has been previously characterised as ground basalt tuff, matching the bulk mineral chemistry and engineering properties of the original lunar soil samples collected by the Apollo missions. Although it is a suitable simulant for conducting research into engineering applications [30], it cannot be claimed to be a typical Lunar regolith analogue since the surface on the Moon does not consist of a single material. Rather lunar soils and they range from anorthositic to basaltic (with a minor meteoritic component of <2%) [31]. Available petrographic studies report the regolith simulant as a multicomponent material consisting of olivine and plagioclase solid-solution phenocrysts, together with pyroxene and titanium-rich magnetite content, incorporated in volcanic glass of an approx. 50% vol. [32]. As such, it represents the five common rock-forming minerals found in the actual material [33].

The as-received regolith, with particle sizes up to approx. 1 mm, was sieved through a laboratory test sieve with 125 µm apertures, in order to ensure a more constant and repeatable particle size distribution and also provide a better flow performance during deposition. The resulting particle size distribution after sieving was: d(0.1): 24 µm, d(0.5): 75 µm and d(0.9):149 µm, as measured via laser diffraction (Mastersizer Sirocco 2000 particle size analyser, Malvern Instruments Ltd., UK). Additionally, the resulting particles also matched the size medians (~60-80 µm) from the sub-millimeter lunar surface soil samples collected

during the Apollo 11-17 and Luna 16-20 missions [31]. Sieving removed approximately 40% wt. of the original sample.

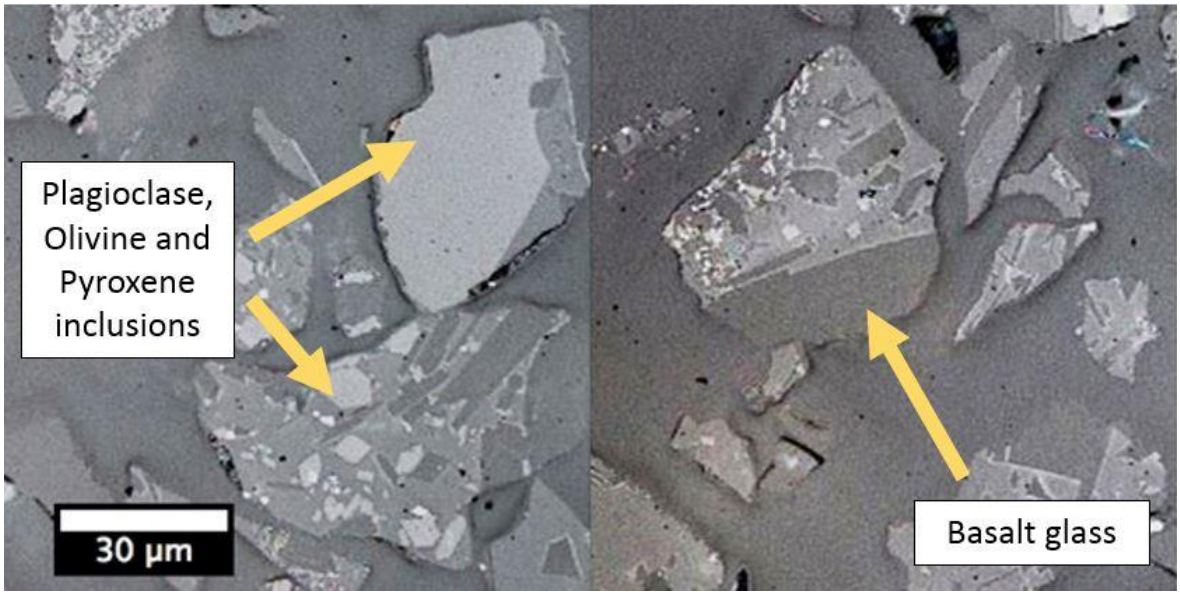

Figure 1 – Bright field optical micrographs showing the multicomponent nature of the granular JSC-1A Lunar mare regolith simulant material, containing various mineral phase inclusions (olivine, plagioclase and pyroxene) in grains of a basalt glass matrix. The scale bar applies to both optical micrographs.

2.2 Additive manufacturing equipment

All powder bed fusion experimentation and manufacturing of test specimens in this study were carried out on a Selective Laser Melting (SLM) machine (SLM100A, Realizer GmbH, Borchen, Germany). The SLM100A was equipped with a continuous wave ytterbium-doped fibre laser (YLR-50, IPG Photonics, Oxford, MA, USA) operating on a central emission wavelength of λ=1.06 µm with a standard TEM_{00} Gaussian beam profile and a maximum indicated power output of 50 W. The SLM100A was equipped with an adjustable beam expander that could deliver a focused beam of 30 – 300 µm in diameter onto the powder bed through a 120 mm f-theta lens. The feedstock material was contained and deposited onto the powder bed through a hopper and spread to a fine layer via a set of recoating blades; **Figure 2.**

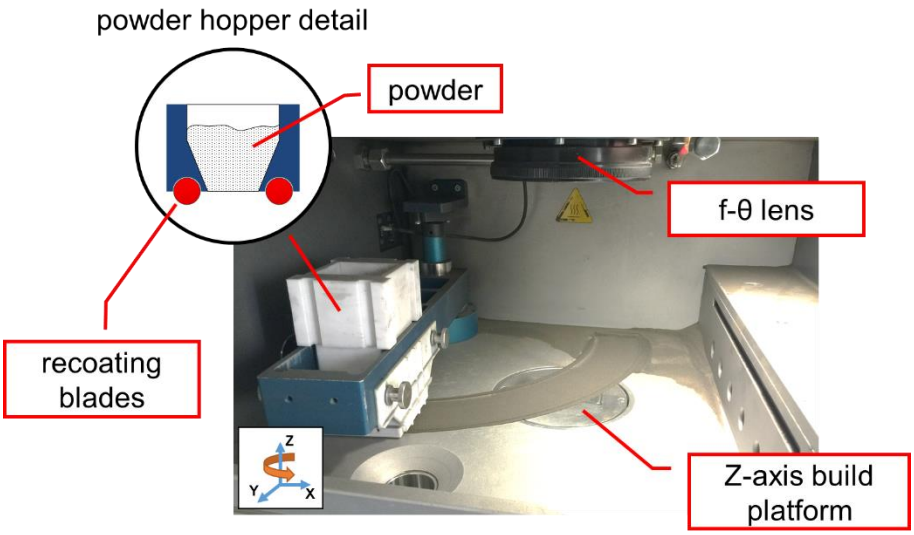

Figure 2 – Detail of the hopper powder deposition mechanism inside the build chamber of the Realizer SLM100A machine

Both single scan track experiments and 3D test geometries were built on a substrate of soda lime glass, **Figure 3**, in order to achieve good bonding of the build geometry to the substrate and avoid unwanted process repercussions (e.g. sample detaching, warping, etc.). The substrate material was chosen due to its matching thermal properties (thermal expansion coefficient, high-temperature working area), optical properties (almost 90% transmissivity at $\lambda = 1.06$ µm) and its relatively low cost. All processing was conducted in an inert environment, purged with argon at 10 mbar overpressure.

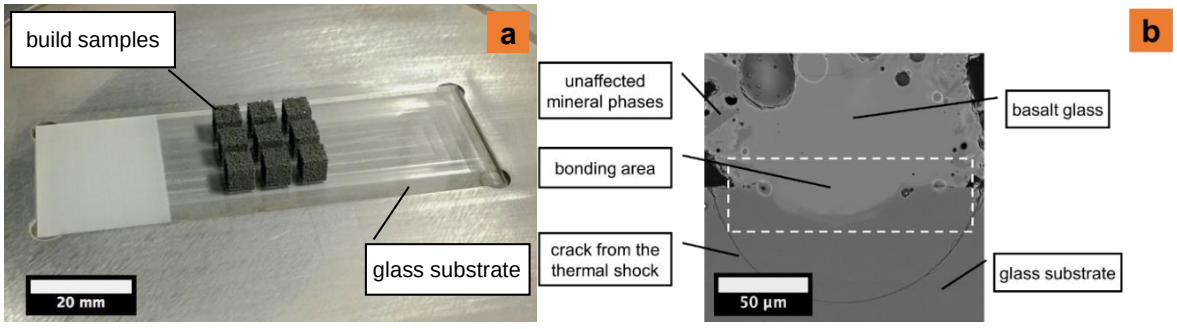

Figure 3 – (a) Additively manufactured 5 mm cuboid samples, built on a borosilicate glass substrate and (b) bonding between the two glass (basalt-borosilicate) materials after laser processing.

More than 130 factors have been identified to affect the process itself and the quality of the parts fabricated via laser melting/sintering [34]. These factors are mainly associated with the

additive manufacturing equipment used, the processing environment and the thermo-physical properties of the feedstock powder material. For this experimental study, the process parameters responsible for the quality of the fabricated test parts were chosen due their importance for controlling the amount of energy required to deliver the laser electromagnetic radiation to the powder bed's surface:

- scanning speed (u), *in mm/s*
- hatch spacing (h), *in µm*
- laser power (P), *in W*
- beam diameter (δ), *in µm*
- layer thickness (t), *in µm*

Because of the inherent characteristics of this particular multicomponent ceramic material, which exhibited a variety of thermo-physical properties including: unusual chemistry, a laser wavelength-dependent absorbance, varying latent heat of fusion, and specific heat between constituents, etc., all of which directly affected its laser sintering profile [35], the optimum energy density to effectively fuse the material was identified through physical experimentation rather than via modelling-based prediction.

During processing, electromagnetic radiation was directed, via the systems optics, onto the powder bed's surface where the focused laser beam formed consecutive bursts of light for a predetermined duration (the beam exposure, in µs) that were spaced apart to achieve a desired exposure distance (in µm) given the speed of movement of the sample. The combination of these two process parameters formed the scanning speed (**Equation 1**) and were responsible for the quality of the single fused tracks formed. The duration of how long

the focused laser beam was focused on a single point will also have momentarily defined the size of the melt pool. A good combination of these parameters could provide a stable melt pool and result in a single track with, ideally, a stable width [36].

Equation 1: $$scanning\ speed\ (m/s) = \frac{point\ distance\ (\mu m)}{beam\ exposure\ (\mu s)}$$

This experimental investigation was conducted in a progressive manner composed of two main parts:

a) In the first stage, the fabrication of single tracks was examined by varying the laser scanning speed parameter and investigating its effect on the morphology and size characteristics of the tracks.
b) The second stage consisted of fabricating multilayer samples by varying the hatch spacing parameter; the latter is the distance from centre-to-centre between two consecutive single tracks that form a monolayer (also known as the scan spacing) [37]. Relative porosity was used as the core indicator for evaluating the impact of the hatch spacing parameter, and its associated energy input, on the materials microstructure, densification mechanisms and the resultant mechanical properties.

In order to simplify the experimental process, the laser power was set at the equipment's maximum value of 50 W and the beam diameter was set at 80 µm, matching the previously recorded particle size median of 75 µm. It was assumed that the material's intrinsic properties would not be affected by the processing being undertaken and hence were considered as fixed parameters throughout the study. Finally, more complex test pieces were also produced using the optimum processing parameters that were determined and are reported in this paper.

2.3 Microstructure

The morphology and size characteristics of the single fused tracks formed were investigated initially via optical microscopy (Eclipse MA200, Nikon Metrology Europe, Netherlands), with the microstructural analysis of the evolution of the optically observed porosity evolution being conducted using scanning electron microscopy, SEM (Hitachi TM3030, Hitachi High Technologies GmbH, Krefeld, Germany).

The relative porosity (%) was measured with the aid of ImageJ and via the use of micrographs of the samples after cross-sectioning perpendicular and parallel to the build direction. Prior to examination, the samples were embedded in epoxy resin (EpoThin2, Buehler, Illinois, USA) and prepared using a standard metallographic approach, with sequential grinding stages using silicon carbide papers of P320 to P4000 grit size, followed by a polishing stage using polishing cloths and a 0.05 μm alumina suspension. To prevent charging during SEM analysis, samples were coated with a gold/palladium alloy in an 80:20 weight ratio, for 60 s at 25 mA using a sputter coater (Quorum Q150T, Quorum, Edwards, Hastings, UK).

5 different test samples were made with each laser energy density value, creating a total of 45 samples for the 9 different laser energy inputs used, **Figure 3.** Images were taken from every sample and they were processed and binarized using a suitable threshold value so that the porosity was clearly visible. The porosity values were subsequently calculated as the ratio of the black to white pixels, which corresponded to the total fraction of pores over the examined surfaces [38–40]. The porosity was correlated with the compressive strength of the 3D printed parts.

The density of the laser-fused samples was measured via gas expansion pycnometry. A helium gas multivolume pycnometer (Micrometritics 1305 Multivolume Pycnometer; Micrometritics Instrument Corporation; Georgia, USA) with calibrated measurement and expansion volumes

was used and the samples' mass was determined using a benchtop microbalance (Mettler-Toledo XA105DU, Mettler-Toledo Ltd, UK). All 45 test samples were measured. The calculated densities were correlated to the previously acquired relative porosity and relative density values.

2.4 Surface characterisation

The effect of the hatch spacing process parameter on the surface texture of the laser fused layer and its influence on part porosity via the effective packing behaviour of the deposited layer in the powder deposition/recoating stage was investigated via infinite focus microscopy (Alicona InfiniteFocus, Alicona Imaging GmbH, Bartlett, IL). Because of the relatively coarse surface profile (evident from visual inspection), a 5x objective lens was used with a resolution setting that could detect features down to a size of 2 µm. An effective area of 4 x 4 mm over the total surface of the 5 mm cuboid samples was examined and the surface texture values given in

Table 1 were calculated by analysing the three-dimensional surface profiles via the equipment's native software, IF MeasureSuite 5.1.

Table 1 – Measured surface characteristics for defining the surface texture of the additively manufactured lunar regolith simulant components.

S_a	Average surface roughness / µm
S_q	Root mean square roughness / µm
S_p	Maximum peak height / µm
S_v	Maximum valley depth / µm

Again, a total of 45 samples were subjected to surface texture analysis representing 5 repetitions out of 9 test samples made with different hatch spacing settings of 170 – 250 μm. All the samples were thermally conditioned at 20 ± 0.5°C and 50 ± 5% relative humidity (RH) for 24 hours prior to examination in order to ensure sample dimensional equilibrium.

2.5 Mechanical properties

The influence of the laser energy input on the mechanical properties of the fabricated samples was investigated by evaluating the compressive strength and hardness of the samples made.

Compressive tests were conducted in accordance to the ASTM C1424-15 standard on a universal dual column testing machine (Instron 3366, Instron, High Wycombe, UK) fitted with a 50 kN static load cell, at a constant crosshead speed of 0.5 mm/min, until failure by crushing occurred. Compressive load and displacement data were recorded in 0.1 second intervals during testing and the maximum load reached was used to calculate the compressive strength of the additively manufactured lunar regolith simulant specimens. The elastic modulus was obtained from the slope of the compressive stress versus strain curve at higher values of stress and strain. Results are reported as the average compressive strength (in MPa) and elastic modulus (also in MPa) as a function of their respective relative porosity (in %). Testing was conducted in laboratory conditions at 23ºC and 55% RH.

Material hardness was measured using the Vickers micro-indentation method, in accordance with the ASTM C1327-15 standard and measured via an automated hardness testing machine (Struers Durascan 70, EMCOtest, Kuchl, Austria). A Vickers diamond indenter was used with a 0.05 kg load and a 15 seconds dwell time. Due to the samples' porous structure, hardness measurements were taken from multiple locations over the test samples' surface in order to

acquire a range of hardness values with a minimum number of five crack-free indentations being required. Specimens were polished as per section 2.3.1 to produce the surface finish required for Vickers micro-indentation. Testing was again conducted in laboratory conditions of 23ºC room temperature and 55% RH relative humidity. Results are reported as an average value of the hardness number $HV_{0.05/15}$ with the accompanying standard deviation.

2.6 Powder bed temperature

The laser-induced evolution of temperature in the powder bed during processing, and its influence in the quality and occurrence of defects in the AM-builds, was investigated by embedding 200 µm diameter, type K thermocouples (R17, Reckmann, Hagen, Germany) in the powder bed and at the base of the build specimen. The temperature data was recorded at 1 millisecond intervals via a data acquisition device (TC-08, Pico Technology, Eaton Socon, UK) throughout the building process, **Figure 4**.

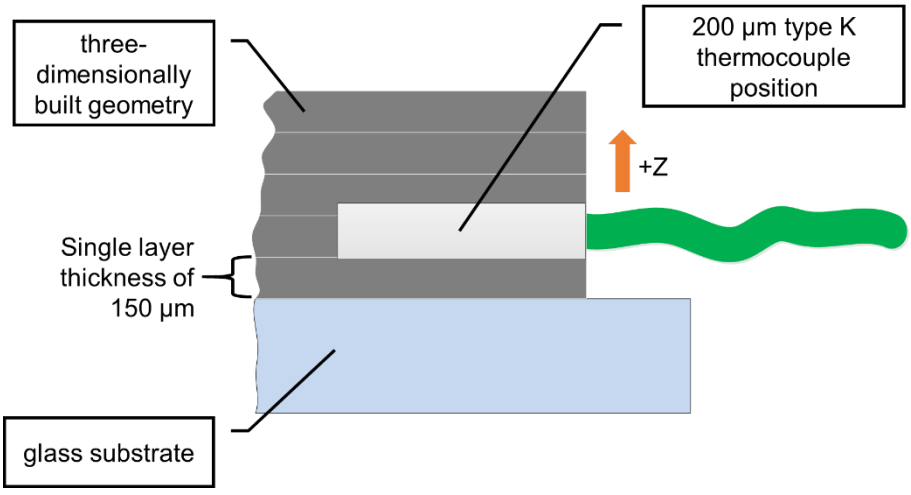

Figure 4 – Schematic of thermocouple embedding and positioning.

3 Results & Discussion

3.1 Layer thickness

The powder used exhibited a unimodal particle size distribution with a particle size median of 75 µm and a maximum particle size of 143 µm, therefore the minimum layer thickness was set to 150 µm. This prevented the largest powder particles from being dragged by the recoating blade, damaging the smoothness of each layer as it was formed [41]. The choice of layer thickness is often guided by the feedstock particle distribution as above and is directly correlated to both the build speed and the resolution the process can achieve. The chosen layer thickness is within the range of conventionally used layer thicknesses for laser based powder bed fusion processes and enables a relatively high resolution but at some cost to the build speed (further discussed in section 3.6).

Sieving of the feedstock materials is conventionally regarded as a profound and process-related necessity for powder bed fusion processes but material sieving on the lunar surface is expected to pose as a considerable challenge for bulk material handling, due to the presence of electrostatic charges in the lunar regolith [42] (further addressed in Section 3.7) thus obstructing the free flow of the feedstock regolith onto the powder bed. Potential mitigation of such an environment/material-related setback could be an integrated sieving system with charge dissipation capabilities. Such a system could potentially contain a metallic/conductive mesh that is connected to ground and would help discharge the existing electrostatic charges of the lunar regolith granular feedstock matter. Due to the low gravity and lack of atmosphere the sieving system could be carried out in a closed system with circulated air to help transporting especially the smaller particles through the sieve.

The choice of layer thickness was considered the starting point for the development of the process parameters since it is directly connected with the laser absorption performance of the powder bed [43] and the optimum energy input required to achieve a temperature above $T_{Solidus}$ and effectively fuse the particles [44] contained in the given volume of material. Any excess or deficiency in the expected energy input would have resulted in unwanted process irregularities during the formation of the single fused tracks [45].

3.2 Single tracks

For the results described here, the layer thickness was kept constant at 150 µm since changes would have affected the volume of material being processed, which would, in turn, have meant that the energy input was changed affecting the likelihood of achieving successful fusion. The results collected from this experimental stage were assessed and then utilised in the fabrication of multilayer test samples.

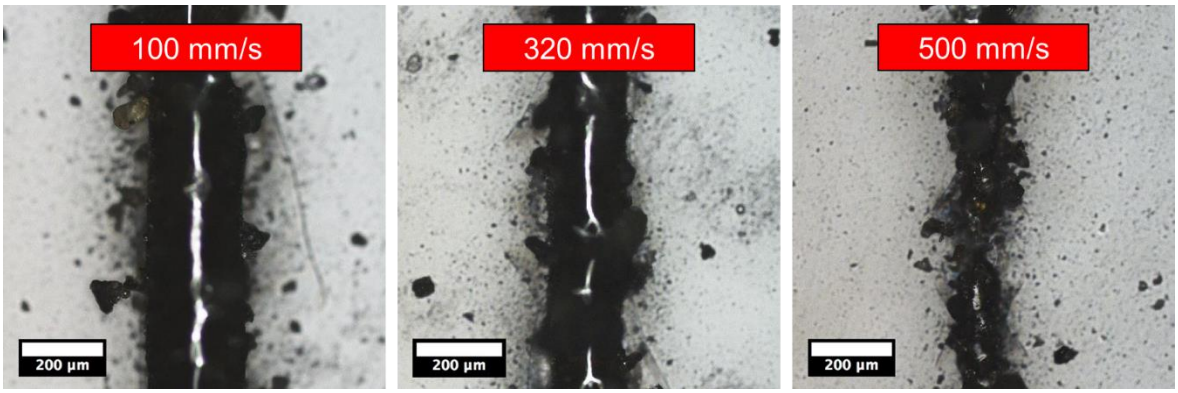

Figure 5 – Optical micrographs showing the morphology and size characteristics of single tracks obtained over a range of different laser scanning speeds.

Figure 5 shows three characteristic types of single tracks obtained over a range of laser scanning speeds:

- The speed setting of 100 mm/s produced an energy density that enabled the successful fusion of a well formed and continuous track of stable width, of approx. 230 ± 20 µm, and

regular morphology. However, it also resulted in some of the powder being 'blown away' from the immediate laser scan area, **Figure 7**. It is assumed that this occurred because the energy input was excessive causing some of the finer particles to vaporise, the resulting gas formed then displaced some of the surrounding powder particles.

- At between 200 – 400 mm/s, single tracks of consistent size and morphology were again observed but the inadvertent powder removal effect was not observed. Tracks made at a speed setting of 320 mm/s were approx. 190 ± 45 μm wide. Note, however, that although the resulting tracks appeared to be continuous, different powder particles could be seen to be adhered to the outer surface of the solidified area of the scan track. These were identified (and are illustrated below in **Figure 6**) as:

    a) Large particles that had not melted but adhered due to the melt pool formed,
    b) Olivine and plagioclase crystals that had also not melted due to their having a significantly higher melting temperature than that generated during laser scanning, and
    c) Other mineral crystal particulates that were partially embedded / incorporated in the melt and were protruding from the solidified single track.

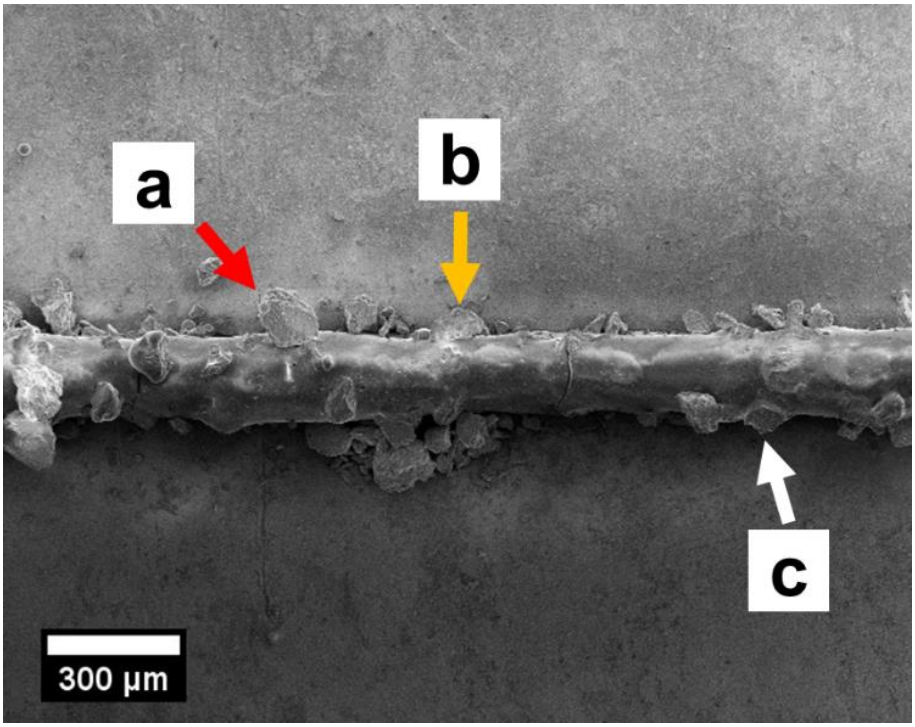

Figure 6 – SEM image showing irregularities formed during laser fusing of single tracks at a laser scanning speed of 320 mm/s.

- Finally, the process speed setting of 500 mm/s provided a relatively low energy input where melting of the powder material could only be achieved at the centre of the track, mainly due to the Gaussian beam profile of the laser and the consequent energy distribution. This resulted in failure to achieve adequate fusion amongst the surrounding particles. This led to a single track of irregular and discontinuous shape and track width measurements yielded values of 100 – 180 µm due to the particles being randomly incorporated into the central fused and solidified region of the track.

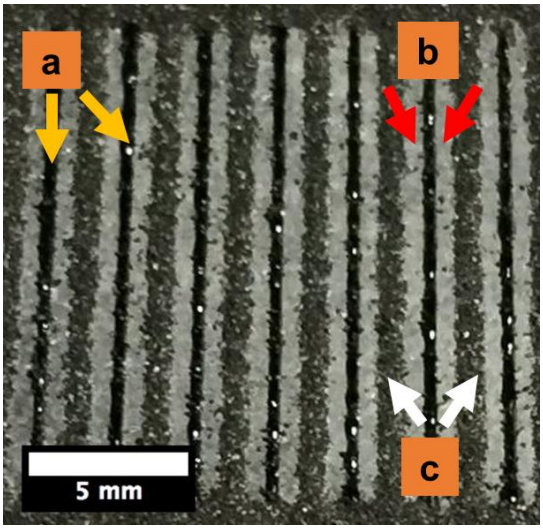

Figure 7 – Example of the result of high intensity energy input on single tracks. (a) single fused tracks, (b) blown powder and (c) unaffected lunar mare regolith simulant powder.

3.3 Multiple layers

Multilayer manufacturing experiments were carried out using a constant scanning speed of 320 mm/s, the value identified as the best by the previous single-track experiments, and by varying the hatch spacing parameter over a range of values from 80 µm, corresponding the width of the laser beam, up to 250 µm.

Energy inputs corresponding to the hatch spacing range 80 – 160 µm, highlighted inside the red dashed box in **Figure 8a**, yielded poor build features and poor reproducibility with >80% failure rate. This was ascribed to excessive energy input and the occurrence of accumulated heat and thermal stress effects during processing, causing the parts to distort and detach from the substrate base.

The range of hatch spacing values between 170 – 250 µm, in the green box in **Figure 8a** and shown separately in **Figure 8b**, yielded successful and highly repeatable three-dimensional geometries, with no apparent macroscopic flaws. As indicated earlier, no samples were made with a value of greater than 250 µm hatch spacing in this study because of their poorly fused nature.

The optimum processing conditions that were identified in this study were subsequently used to manufacture a range of more complex geometries, including engineering components, fine lattices, etc., as seen in **Figure 17** in order to showcase the level of process control that had been achieved.

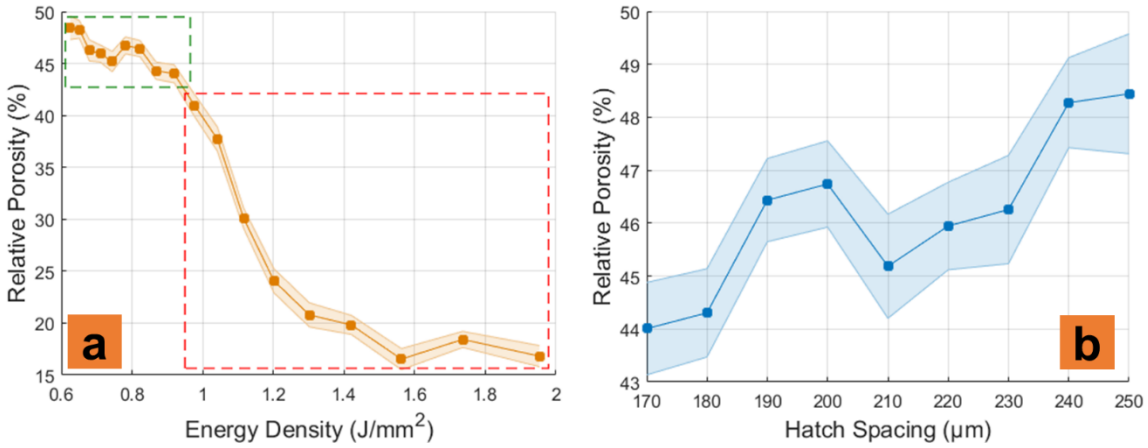

Figure 8 – Influence of (a) laser energy density between 0.6 – 2 J/mm^2 and (b) hatch spacing between 170 – 250 µm, on test samples' relative porosity. The shaded areas represent the standard error.

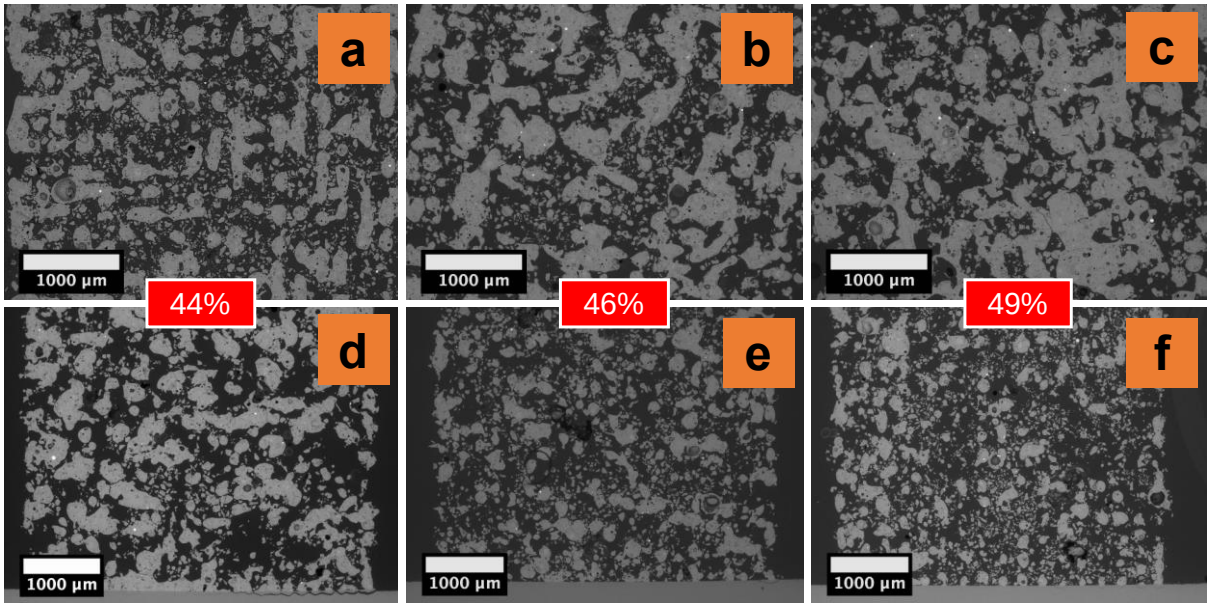

Figure 9 – SEM micrographs (a-c) are top down and (d-f) is the accompanying side view of the cross-sectioned samples. Images show the inherently porous microstructure of the laser additively manufactured test samples, processed with 50 W laser power, 320 mm/s scanning speed and 170 µm (a, d), 210 µm (b, e) and 250 µm (c, f) hatch spacing.

Porosity measurements conducted via digital processing of the SEM micrographs, **Figure 9**, revealed the correlation of the hatch spacing parameter to the resulting porosity. As seen in

Figure 8, a range of 44 – 49% relative porosity was measured over the 170 – 250 µm hatch spacing values used, with a lower hatch spacing yielding less porosity as expected. The density was improved by the higher energy density delivered to the surface of the powder bed.

In a similar manner, measurements recorded via gas expansion pycnometry showed an almost identical correlation of the hatch spacing parameter to the samples' density as measured by pycnometry, with values ranging from 1.76 – 2.3 g cm^{-3} over the 170 – 250 µm hatch spacing values used. The plot overlay in **Figure 10** shows the samples' densities as measured by the two approaches (where the relative density is calculated as 100 – the relative porosity in percent). Additionally, the density results achieved are comparable to those obtained from conventional sintering; Meurisse et al obtained a value of 2.253 g cm^{-3} after HIP processing of JSC-1A lunar mare regolith simulant in air [46].

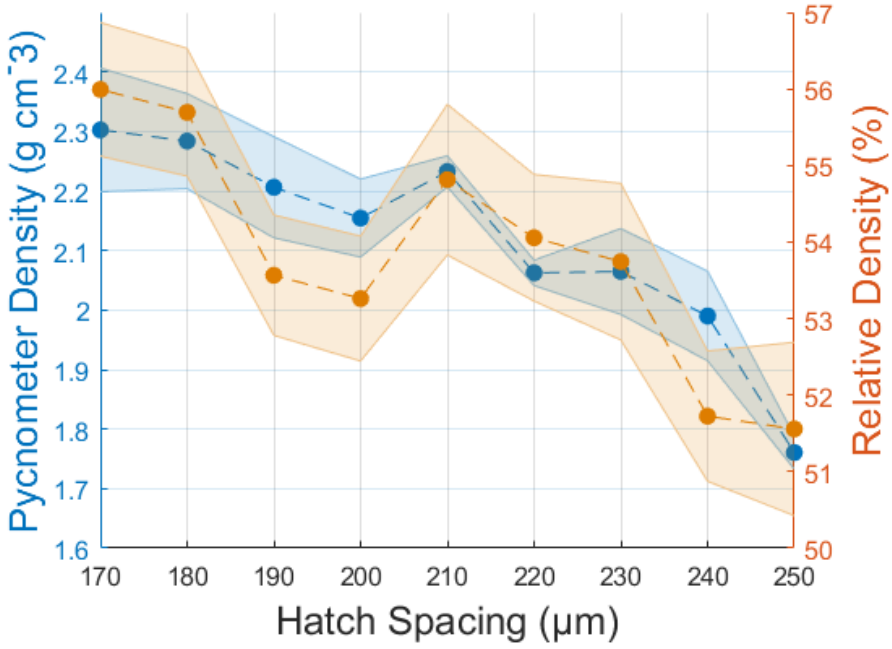

Figure 10 – Comparison of measured 3D printed samples densities as measured using pycnometry and from the relative porosity values obtained by SEM analysis. The shaded areas represent the standard error.

3.4 Surface characterisation

The formation of a smooth surface after each layer has been formed during the fabrication process is essential for the powder packing and can influence the porosity and in the mechanical strength. Close examination of the influence of hatch spacing on relative porosity in **Figure 8b** revealed that in the range between 200 – 230 µm there was a small unexplained reduction in porosity from 47% to 45%. The authors theorise that this 2% porosity reduction was caused by an improvement in the surface texture of the processed layer. **Figure 11** shows three-dimensional surface profile measurements gathered via infinite focus microscopy and shows the evolution of surface texture over an area of different hatch spacing settings, from 170 – 250 µm. It is known that non-spherical particles, such as the JSC-1A lunar regolith simulant, tend to mechanically interlock together due to their angular and sub-angular morphology. This creates powder layers with inhomogeneous packing densities [37]. The resulting intergranular and intragranular voids – a common packing characteristic of both actual and simulated lunar regolith [31] – between the powder layers, result in the formation of defects within the solid layer surface, causing partial melting and porosity. The latter is likely to have been made worse by the different melting temperatures of the various crystalline mineral phases in the regolith. The lowest average surface roughness value of 71 µm and root mean square roughness value of 93 µm were recorded at the hatch spacing setting of 210 µm, where the reduction in porosity was previously identified. It is suggested that this is an effect caused by a reduction in surface abnormalities due to melt pool overlaps or protruding particles**, Figure 12.** This also matches the results from the measurements of the maximum peak heights (S_p). It should also be noted that past the hatch spacing setting of 230 µm, there was a significant increase in the maximum recorded valley depths (S_v), explaining the increase in porosity as a result of the large pore channels formed in between the scanned tracks.

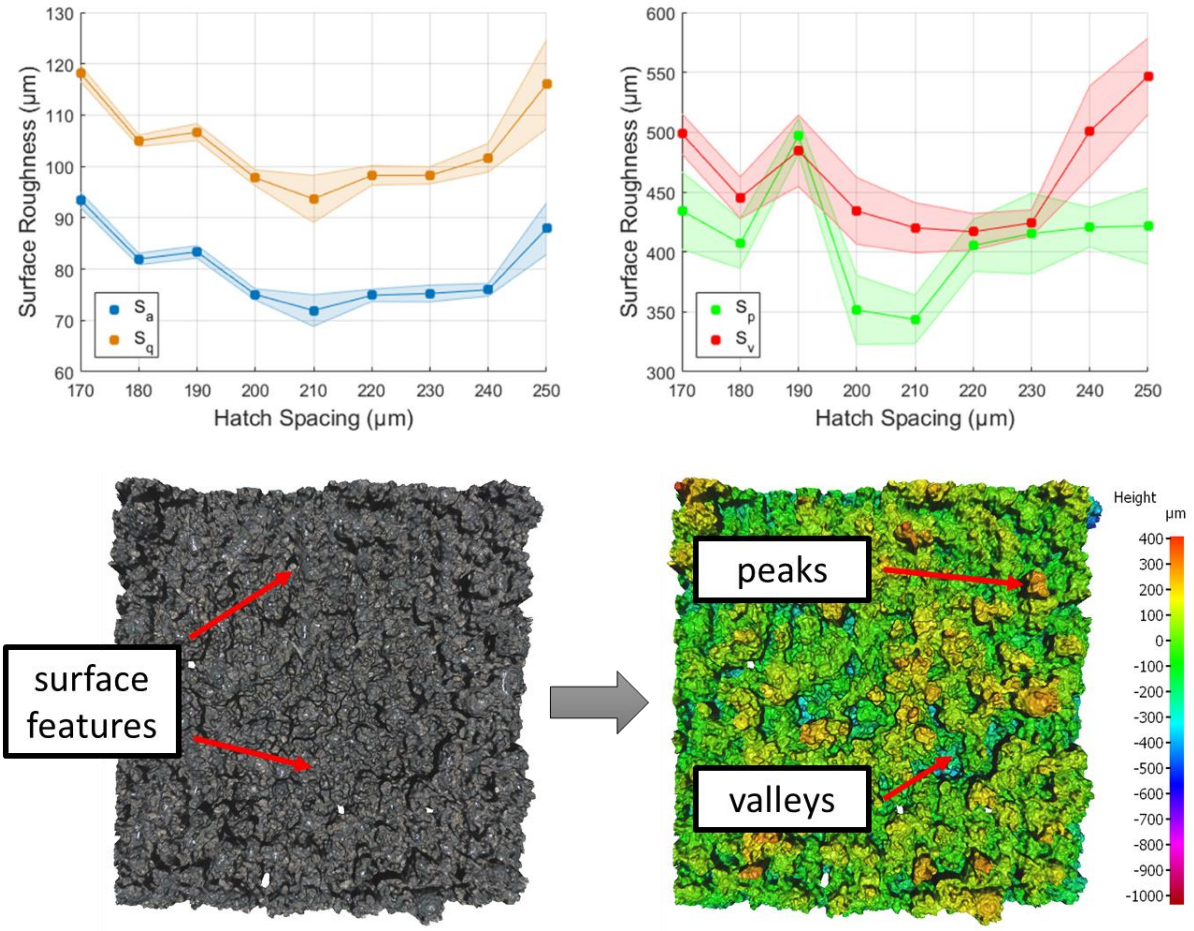

Figure 11 – Top: Influence of hatch spacing on the surface roughness of laser processed layers. Bottom: Example of a three-dimensional surface profile (top-down view) from an additively manufactured lunar regolith simulant part, acquired via surface profilometry via the Alicona Infinite Focus microscope. The shaded areas represent the standard error.

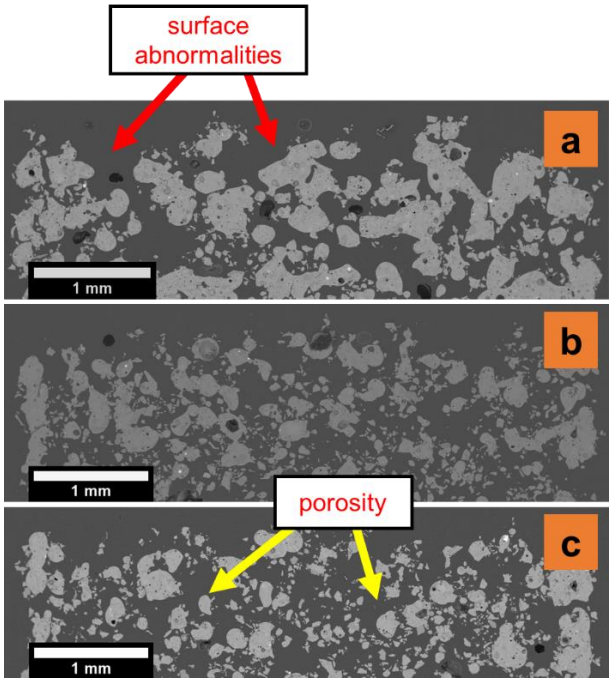

Figure 12 – SEM image cross-sections showing the evolution of porosity and surface abnormalities due to the change of hatch spacing. Samples built with a)170 µm b) 210 µm and c) 250 µm hatch spacing settings.

As expected hatch spacing is a contributory factor in the resultant surface quality. A previously consolidated single layer with reduced surface roughness, is likely to result in smooth deposition and packing of the next, fresh powder layer, which, in turn, will benefit the densification of the material via more effective interlaminar fusing [45,47,48].

3.5 Microstructure

The microstructure of a powder bed fusion additively manufactured part made from a multicomponent ceramic material such as the lunar regolith simulant is very different from a typical engineering ceramic material, even when it is built with the same AM technique.

When selectively scanned by the laser beam, the powder particles in each layer undergo rapid melting, with solidification of the resultant melt pool. What might be expected to be seen, therefore, is a microstructure not too dissimilar to that of a vitrified clay body of similar composition.

The regolith materials' inherent composition comprises primarily of silicate minerals, including plagioclase feldspars, olivine, pyroxene, and others [22], that when heated and then cooled rapidly over a critical rate of 52°C/min can result in glass formation [19]. This increases the already high glass content, favoring vitrification-based densification mechanisms. However, as a result of the particles' angular morphology and consequent poor packing, the powder bed contains significant porosity that causes the laser beam to be unevenly dispersed. In addition, it is likely that there will have been a degree of partial absorption of some of the incident energy by the lower layers [49] and it was observed that nearby unmelted particles were often attracted to the melt pool by capillary forces. The combination of these undesirable effects will have acted as contributory factors against successful densification, resulting in the very low-density bodies being formed. In conventional vitrification of ceramics densities well in excess of 90% of theoretical are usually achieved [50]

Measurements from the evolution of temperature in the powder bed during processing have revealed both an apparent maximum temperature of <500°C and cooling rates of up to 10^5°C s^{-1} as shown in **Figure 13**. Although the former is well below the melting temperature of any of the regolith simulant's constituents, it is suggested that the temperature recorded by the thermocouple will have been a mean value, rather than the local peak value. The effect of the very high cooling rate will have been to encourage the formation of more glass as outlined above. In the likelihood of carrying out such a processing task in the hard-vacuum atmosphere of the lunar environment, the cooling of rates post laser irradiation, are expected to be less due to the different heat dissipation mechanisms taking place and thus leading to a reduced glassy content when compared to terrestrial conditions processing. This is further discussed in section 3.7.

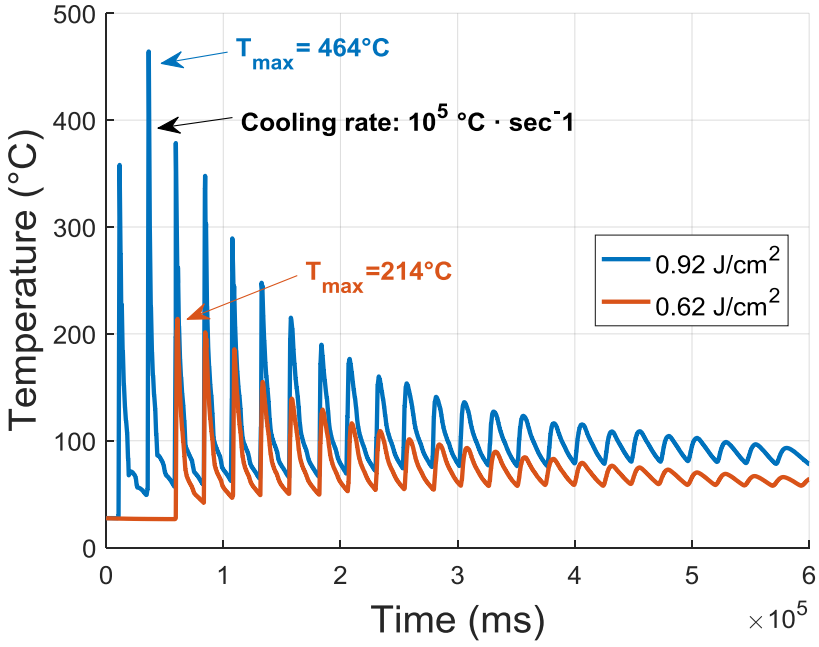

Figure 13 – Evolution of powder bed temperatures during laser irradiation with two different laser energy density settings. Temperature data was acquired by embedding 200 µm, Type-K thermocouples inside the powder bed.

Whilst processing of the regolith powder (e.g. grinding it to make it finer and adding sintering/fusing aids) could well have yielded greater densification, the object of this study was to see what could be achieved with the as-received regolith.

3.6 Mechanical properties

The mechanical properties of the test samples were evaluated via compression and micro-hardness testing. Results revealed that the build structures were able to sustain loads up to 500 N, **Figure 14**, with average compressive strength values ranging from 0.2 ± 0.04 MPa up to 4.2 ± 0.1 MPa and **Figure 15,** average modulus of elasticity values of 41.7 ± 6.7 MPa up to 287.3 ± 6.4 MPa.

The shapes of the compressive stress / strain curves in **Figure 14** are typical of the behaviour of porous, brittle materials such as ceramic foams, cellular ceramics [51,52] and porous concrete [53]. In each case there was a steady but non-linear increase in stress up to a rounded maximum when the body started to crush. Failure was subsequently non-catastrophic. Apart from the

curve obtained at the lowest laser energy density, 0.63 J/mm^2, the curves formed a steady progression with a low stiffness at low stresses and strain that increased at higher values. The greater the laser energy density used, the greater the stress and strain that could be tolerated before the onset of crushing of the walls between the pores.

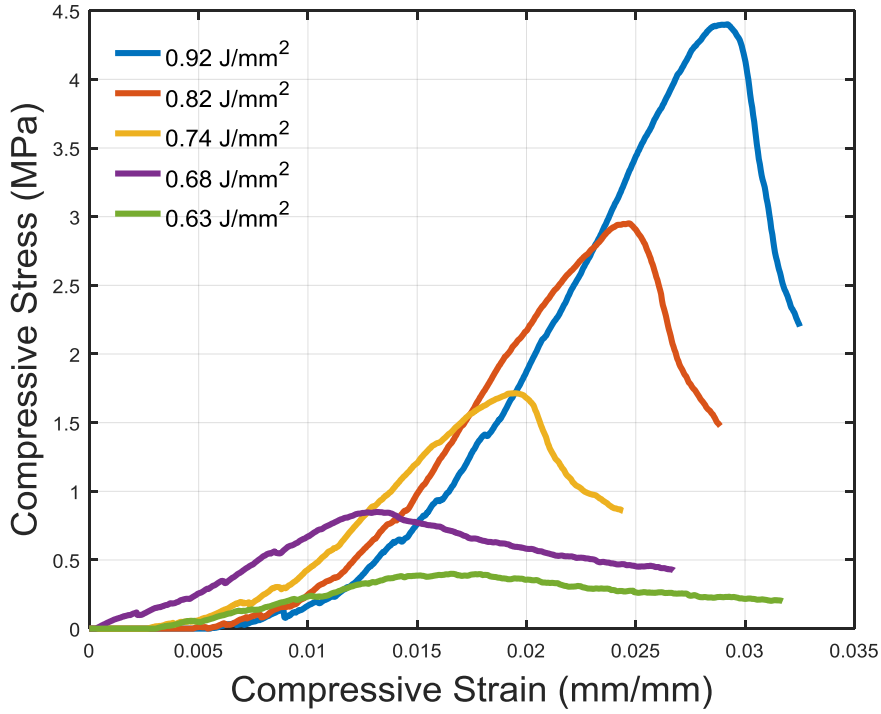

Figure 14 – Example of a compressive stress vs. compressive extension graph, recorded during mechanical testing of additively manufactured parts from JSC-1A mare lunar regolith simulant.

Figure 15a shows the relationship between the porosity and the compressive stress and elastic modulus. Two observations can be made. First, how similar the shapes of the two curves are, something that is not unexpected given the link between the parameters. Second, how although there is a clear trend that lower porosity led to greater strength and elastic modulus, as expected, at around 46% porosity there was a high degree of scatter in the values obtained. Since higher laser densities led to greater compressive strength but little difference in porosity, it is assumed that the effect was to create denser struts between the pores due to greater melting.

This is supported by the plot of compressive strength and elastic modulus against laser energy input; a clear and almost linear correlation was observed, **Figure 15b.**

Equation 2 [37,51–53] expresses the energy density applied to the surface of the powder bed; it was used to link the combination of process parameters, including laser power (P), scanning speed (u) and hatch spacing (h), with the energy density (E).

$$\textit{Equation 2: } E = \frac{P}{u \cdot h} \ (J/mm^2)$$

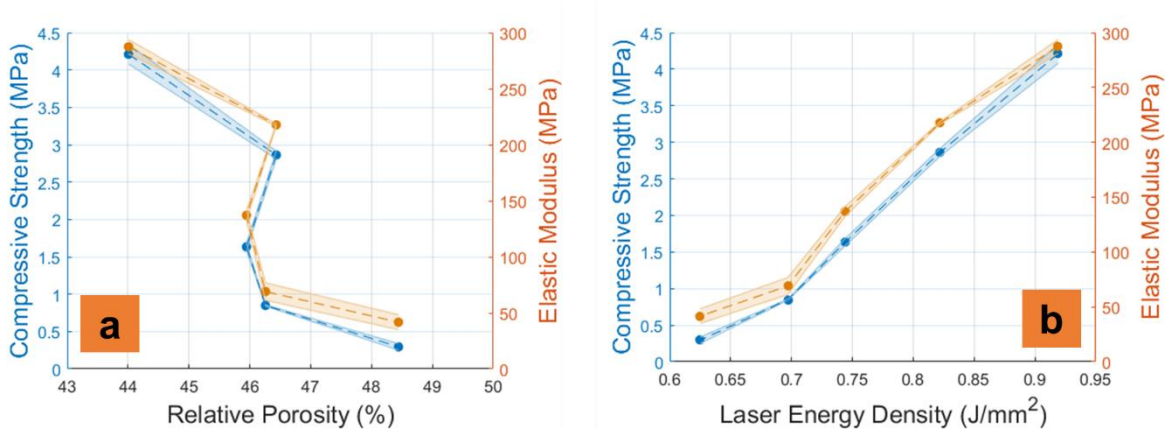

Figure 15 – Influence of relative porosity (%) and energy density on the compressive strength and elastic modulus of additively manufactured parts from lunar regolith simulant. The shaded areas represent the standard error.

The compressive strength and elastic modulus measured in this study are to the best of our knowledge the first ever reported values for additively manufactured lunar regolith simulant structures fabricated without additives, only using heat, thereby satisfying the concept of ISRU, where in principle only on-site available resources are to be used. The mechanical strength is sufficient for low stress applications such as the particle filter illustrated in **Figure 17b** as well as for bulk construction and suggests that powder bed fusion processes can be used to form engineering materials from lunar regolith without additives.

The assessment of a material to be used as a load bearing structural element relies upon its ability to withstand the loads likely to be imposed on it; in the case of a building on the Moon

where there will not be any storms since there is no atmosphere, this will effectively be the load imparted by its own mass. Note that this will be also much lower than it would be on earth due to the Moon's low gravity, approx. 1/6 of that on Earth [54].

The maximum compressive strength recorded in the current work was approx. 4.2 ± 0.1 MPa and corresponded to a laser energy density of 0.9 J/mm^2. This value is slightly higher than the 3.65 MPa obtained by Contour Crafting [55], another 3D printing method which uses additives. Both approaches, however, yielded much lower strengths than those obtained from regolith-based concretes also using process additives [56] or when conventional sintering techniques were used [46,57] where values ranging from 36 up to 150 MPa were recorded. It should be noted, though, that both these manufacturing routes require significant additional resources, whether equipment and/or materials, making them a more significant technical challenge to locate and operate on the Lunar surface.

Nevertheless, the strength obtained in the present work is comparable to the minimum compressive strength value of 3.5 MPa for common masonry clay bricks (BS 6073). When the effect of the lower gravity is taken into account the performance would be equivalent to approx. 25 MPa here on earth, i.e. the additively manufactured regolith would be as effective in terms of strength as the standard concrete building blocks used in terrestrial structures [58]. Therefore, it is concluded that the strength achievable with the regolith AM components is likely to be sufficient for the construction of even quite large structures on the lunar surface. The build speed for the process parameters used in this study would likely not be suitable for bulk construction. The process optimized in this study was aimed at finding the mechanical properties for a laser based powder bed fusion process of lunar regolith and was not optimized for build speed. For the large scale, low resolution prints needed for construction the layer height and laser energy density could be increased which would improve the build

speed significantly, at the cost of lower resolution and coarser build features. The mechanical strength of the large-scale prints would likely be similar to the values reported here for the same level of porosity, although only further experimental work could verify this.

Furthermore, it may be possible to avoid the sieving process completely if the layer height is greater than the largest particles, given that the laser penetration depth is high enough to allow for consolidation between the layers. Un-sieved regolith may have reduced flowability and a feedstock delivery system less reliant on good flowability could be used. The SLM manufacturer, Realizer, has already designed such a system. However, the mechanical strength of structures build by SLM of un-sieved regolith is likely to be different due to the bimodal particle distribution, which affects the packing density.

Material hardness measurements revealed that laser energy density (in the range where geometrically stable samples were built) had minimal effect on the performance, **Figure 16**. A range of 735-603 $HV_{0.05/15}$, with an average value of 657 ± 14 $HV_{0.05/15}$, was recorded; this is comparable to, and slightly better than, borosilicate glass at ≈ 580 HV, a glass used in various industrial and domestic applications due to its very low thermal expansion.

As indicated earlier, the optimum processing conditions were used to manufacture a range of more complex geometries, these are shown in **Figure 17**. These show the ability to achieve fine features, which may open up the potential to achieve more than simply the manufacture of simple structural components for buildings. Example of such a demanding geometry could potentially be bespoke air filters; their function would not only rely on the shape of the screening components but also on the path of the airflow (also in **Figure 17b**).

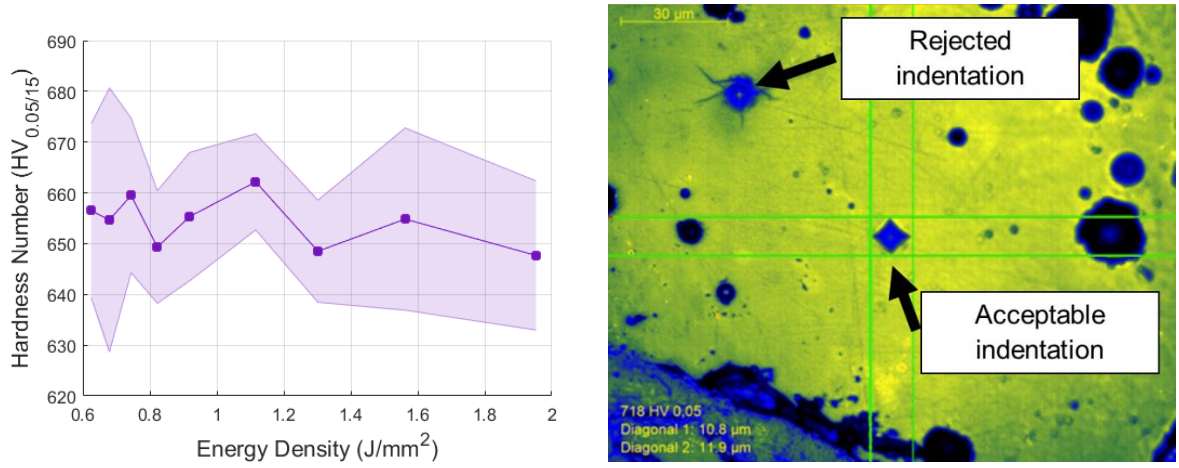

Figure 16 – Influence of energy density on the hardness of additively manufactured parts from lunar regolith simulant (left). Example of indentations made across the surface of additively manufactured lunar regolith simulant test samples (right). The shaded areas represent the standard error.

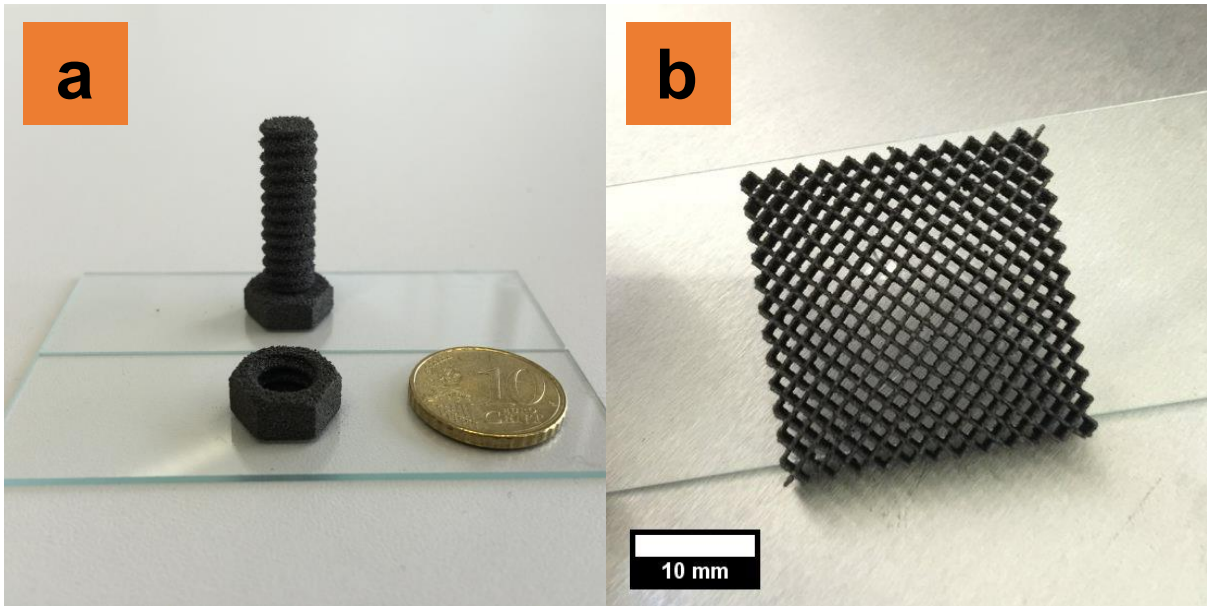

Figure 17 – Examples of laser additively manufactured parts from lunar mare regolith simulant JSC-1A (a) M8x25 bolt (next to a 10-cent coin) – print time approx. 1 hour 45 mins, (b) example of a lattice structure to be used as a dust/particle filter -print time approx. 15 mins.

3.7 Influence of lunar environment on powder bed fusion processing

Although this experimental study consisted of a preliminary investigation into the feasibility of using fusion bed additive manufacturing of lunar regolith simulant and the work was obviously conducted under terrestrial processing conditions, the authors would like to add a brief commentary section discussing the probable influence of undertaking such manufacture under lunar conditions using actual lunar regolith. In particular, the comments relate to potential areas of concern should it ever be planned to use laser-based powder bed fusion on the Moon.

Atmosphere: The extremely thin lunar atmosphere of helium, nitrogen, argon and hydrogen exists at a very low concentration, just $2x10^5$ molecules cm^{-3}, some 14 orders of magnitude lower than that on earth [59]. This is expected to result in contamination-free processing, eliminating the possibility of adsorbed gases and hence resulting in higher surface energies that should promote greater cohesive Van der Waal forces between the particles [55,60] when entering the liquid phase during laser melting. As previously highlighted by *Lim et al*., the significant lack of atmosphere on the lunar surface is also expected to have a strong contribution into heat dissipation mechanisms. As opposed to terrestrial conditions in which heat is propagated via the conduction and convection principles, radiations is expected to be the predominant head dissipation mechanism which is known to be less effective [42].

Gravity: Although the six times lower gravity is beneficial in terms of significantly reducing the strengths required of building materials, it is expected to have a negative impact on both the flow of the powder during processing (flow is expected to be less favourable [28]) and on the active densification mechanisms (densification will be based more on capillary action and

less on sedimentation, which is directly influenced by gravity). Thus, any lunar ISRU-based processes should be specifically designed to be used in a low gravity environment; this would probably involve developing alternative powder feeding/deposition methods that do not rely solely on gravity.

Electrostatics: In addition to the increased cohesiveness of the material due to reduced gravity, the electrostatic loads that exist amongst the lunar regolith particles, due to the ultraviolet photoelectric emissions of solar rays [33], will substantially increase the antiparticle forces, contributing towards a more cohesive behaviour and result to poor flowability of the feedstock material.

Meteoroids: The high impact velocities achieved during the various micro-/meteoroid impacts on the lunar surface, that are also responsible for the formation of the fine-grained powder layer known as regolith, cause localised glassy melts of irregular size and morphology. These melts are known as agglutinates [61] and because of their complex external morphology tend to mechanically interlock with each other. This interlocking is expected to reduce a) powder packing and b) powder flow performance.

4 Conclusions

This project has investigated the processing conditions required and the subsequent mechanical behaviour of the parts fabricated, via adopting laser-based powder bed fusion additive manufacturing for JSC-1A lunar mare regolith simulant powder. The major findings are summarised in the following points:

- As expected, laser energy input, as a result of the combination of process parameters, has a direct effect on the quality of single tracks and the microstructure of the multilayer test geometries. It is important not to use too high a power, which can result in vaporisation of some particles, blowing others away from the laser beam, or too low a power, which results in a failure to achieve fusion of the particles. Identification of an optimum energy input is likely to vary based on equipment specifics and environmental factors, however the parameters that achieve adequate samples with the minimum energy should be regarded as the optimum for lunar regolith simulant structures. This is due to the respective powder bed fusion (PBF) equipment intended for operation in such an extremely limited resource environment as the Lunar surface and hence 'sufficient for task' should be the goal.
- The laser scanning speed is directly influenced by the above arguments; the work here has indicated that a value of 320 mm/s yielded single tracks of stable width and good morphological characteristics. Successful realisation of optimal processing parameters for single tracks is crucial during process development, since it is the basis for allowing mono- and multi- layer fabrication using the lunar regolith simulant feedstock and virtually any laser-based powder bed fusion equipment.

- The hatch spacing was observed to be a critical factor that influenced the surface quality; when not optimised it hindered the optimum deposition of powder layers, which, in turn, negatively affected the resulting porosity. Specifically, hatch spacing settings from 170 – 250 µm resulted in successful and repeatable three-dimensional geometries with no macroscopic build failures and with a final measured porosity of 44 – 49% and density of 1.76 – 2.3 g cm^{-3} as measured by pycnometry. Further work is needed to see if these properties can be improved.
- An analysis of the stress-strain curves recorded during uniaxial compression testing of the additively manufactured lunar regolith simulant samples showed a behaviour similar to cellular structures, such as ceramic foams and porous concrete. The rate of increase in the stress was initially lower than of the strain, but subsequently increased faster at higher loads. Failure was gradual and based on the progressive collapse of the struts between the interconnected porosity.
- Surprisingly, the laser energy input had a direct and linear effect on the mechanical performance of the additively manufactured structures. It is assumed that this was a result of the increase in strength of the struts between the pores even though the porosity level itself was not significantly altered between energy density values of 0.68 to 0.82 J/mm^2. The maximum average compressive strength value measured was 4.2 ± 0.1 MPa and the highest average elastic modulus value was 287.3 ± 6.7 MPa; both were obtained using an energy input value of 0.92 J/mm^2. The strength value is comparable to that of a common masonry brick and so should be adequate for fabricating structural components or relevant replacement parts on the Moon, especially given the absence of storms, and the low gravity.

- The laser-based PBF process was able to deliver results that had a slightly enhanced mechanical performance compared to samples produced via another 3D printing-based processes deemed potentially suitable for other planetary surface manufacturing, but could not outperform those produced with conventional manufacturing techniques, such as conventional sintering in air/vacuum etc. This is likely to be caused by the extent of the residual porosity. However, the laser based PBF process shows good potential due to the ability to utilise lunar regolith simulant after only an initial sieving. In addition, although an enclosed chamber and argon atmosphere was used in the present work, this would probably not be necessary in the lunar environment.
- The layer height used in this study is typical for the PBF process but the resulting print time for larger physical assets, such as the ones required for construction or infrastructure purposes (i.a a dust shield, a pavement block, etc.) would be significant. However, the use of bigger layer thicknesses combined with an increased thermal input, would reduce 3D printing time, of course at the expense of accuracy and coarse features.
- Finally, data such as that generated in this work will enable engineers to simulate, optimise and better design future potential structures that will help maintain and sustain any future human activity on the lunar surface.

Acknowledgments

The authors would like to thank the experimental officers in Loughborough Materials Characterisation Centre (LMCC) and Wolfson School Metrology laboratory for their assistance.

5 References

1. ISECG. The Global Exploration Roadmap. 2013; 50.
2. Sanders GB, Larson WE. Progress Made in Lunar In Situ Resource Utilization under NASA ' s Exploration Technology and Development Program. *J Aerosp Eng* 2013; 26: 5–17.
3. Ceccanti F, Dini E, De Kestelier X, et al. 3D printing technology for a moon outpost exploiting lunar soil. *61st Int Astronaut Congr Prague, CZ, IAC-10-D3* 2010; 3: 1–9.
4. Faierson EJ, Logan K V., Stewart BK, et al. Demonstration of concept for fabrication of lunar physical assets utilizing lunar regolith simulant and a geothermite reaction. *Acta Astronaut* 2010; 67: 38–45.
5. Kading B, Straub J. Utilizing in-situ resources and 3D printing structures for a manned Mars mission. *Acta Astronaut* 2015; 107: 317–326.
6. Khoshnevis B, Bodiford M, Burks K, et al. Lunar Contour Crafting - A Novel Technique for ISRU-Based Habitat Development. In: *43rd AIAA Aerospace Sciences Meeting and Exhibit*, pp. 1–12.
7. Mueller RP, Howe S, Kochmann D, et al. Automated Additive Construction (AAC) for Earth and Space Using In-situ Resources. In: *Proceedings of the Fifteenth Biennial ASCE Aerospace Division International Conference on Engineering, Science, Construction, and Operations in Challenging Environments (Earth & Space 2016)*. American Society of Civil Engineers, Reston, Virginia, USA.http://oro.open.ac.uk/id/eprint/45865 (2016).
8. Crawford IA. Lunar resources: A review. *Prog Phys Geogr* 2015; 39: 137–167.
9. Kallerud M, Nguyen B, Paladin T, et al. In-Situ Resource Utilization: Investigation of Melted Lunar Regolith Simulant JSC-1A. 2009; 1–10.
10. Balla VK., Roberson LB, O'Connor GW, et al. First demonstration on direct laser fabrication of lunar regolith parts. *Rapid Prototyp J* 2012; 18: 451–457.
11. Goulas A, Friel RJ. 3D Printing with Moondust. *Rapid Prototyp J* 2016; 22: IN PRESS.
12. Goulas A, Harris RA, Friel RJ. Additive manufacturing of physical assets by using ceramic multicomponent extra-terrestrial materials. *Addit Manuf* 2016; 10: 36–42.
13. Fateri M, Gebhardt A. Process parameters development of selective Laser Melting of lunar regolith for on-site manufacturing applications. *Int J Appl Ceram Technol* 2015; 12: 46–52.
14. Taylor LA. Status of lunar regolith simulants - An update. *Lunar Explor Anal Gr* 2015; 2012–2013.
15. Rickman D, Edmunson J, McLemore C. A Functional Comparison of Lunar Regoliths and Their Simulants. *J Aerosp Eng* 2012; 9276: 172.
16. Stoeser D, Wilson S, Rickman D. *Design and Specifications for the Highland Regolith Prototype Simulants NU-LHT-1M and -2M*. 2010.
17. Wallace WT, Phillips CJ, Jeevarajan AS, et al. Nanophase iron-enhanced chemical reactivity of ground lunar soil. *Earth Planet Sci Lett* 2010; 295: 571–577.
18. Street, Jr. KW, Ray C, Rickman D, et al. Thermal Properties of Lunar Regolith Simulants. *Eng Sci Constr Oper Challenging Environ 12th Earth Sp 2010 March 1417* 2010; 16p.
19. Ray CS, Reis ST, Sen S, et al. JSC-1A lunar soil simulant: Characterization, glass formation, and selected glass properties. *J Non Cryst Solids* 2010; 356: 2369–2374.

20. Pinheiro AS, da Costa ZM, Bell MJV, et al. Thermal characterization of glasses prepared from simulated compositions of lunar soil JSC-1A. *J Non Cryst Solids* 2013; 359: 56–59.
21. Liu Y, Taylor LA. Characterization of lunar dust and a synopsis of available lunar simulants. In: *Planetary and Space Science*. Elsevier, 2011, pp. 1769–1783.
22. He C. *Geotechnical Characterization of Lunar Regolith Simulants*. Case Western Reserve University, 2010.
23. Rickman DL, Stoeser DB, Benzel WM, et al. Notes on Lithology, Mineralogy, and Production for Lunar Simulants.
24. Allan SM, Merritt BJ, Griffin BF, et al. High-Temperature Microwave Dielectric Properties and Processing of JSC-1AC Lunar Simulant. *J Aerosp Eng* 2013; 26: 874–881.
25. Dąbrowski A, Mendyk E, Robens E, et al. Investigation of surface properties of lunar regolith part III. *J Therm Anal Calorim* 2008; 94: 633–639.
26. Ettouney MMM, Benaroya H. Regolith mechanics, dynamics, and foundations. *J Aerosp Eng* 1992; 5: 214–229.
27. Gualtieri T, Bandyopadhyay A. Compressive deformation of porous lunar regolith. *Mater Lett* 2015; 143: 276–278.
28. Walton OR, Moor CP, Gill KS, et al. Effects of gravity on cohesive behavior of fine powders: Implications for processing Lunar regolith. *Granul Matter* 2007; 9: 353–363.
29. Edmunson J, Betts W. NASA lunar regolith simulant program. *Lunar Planet* …http://adsabs.harvard.edu/abs/2010LPI....41.1786E (2010).
30. Taylor LA, Pieters CM, Britt D. Evaluations of lunar regolith simulants. *Planet Space Sci* 2016; 1–7.
31. Mckay DSDS, Heiken G, Basu A, et al. The lunar regolith. *Lunar Source B A User's Guid to Moon* 1991; 285–356.
32. Hill E, Mellin MJ, Deane B, et al. Apollo sample 70051 and high- and low-Ti lunar soil simulants MLS-1A and JSC-1A: Implications for future lunar exploration. *J Geophys Res E Planets* 2007; 112: 1–11.
33. Medrano-E'Vers A, Morales-Hernández AE, Valencia-López R, et al. *Enfermedad granulomatosa crónica*. 2017. Epub ahead of print 2017. DOI: 10.1007/s13398-014-0173-7.2.
34. Rehme O, Emmelmann C. Rapid manufacturing of lattice structures with selective laser melting. In: Bachmann, Friedrich G.; Hoving, Willem; Lu, Yongfeng; Washio K (ed) *Proceedings of the SPIE: Laser-based Micropackaging*, pp. 192–203.
35. Upadhyaya GS. Some issues in sintering science and technology. *Mater Chem Phys* 2001; 67: 1–5.
36. Yadroitsev I, Gusarov a., Yadroitsava I, et al. Single track formation in selective laser melting of metal powders. *J Mater Process Technol* 2010; 210: 1624–1631.
37. Brandt M. *Front Matter*. 1st ed. Woodhead Publishing. Epub ahead of print 2017. DOI: 10.1016/B978-0-08-100433-3.01001-0.
38. Carter LN, Essa K, Attallah M. Optimisation of Selective Laser Melting for a high temperature Ni superalloy. *Rapid Prototyp J*.
39. Monroy K, Delgado J, Ciurana J. Study of the pore formation on CoCrMo alloys by selective laser melting manufacturing process. *Procedia Eng* 2013; 63: 361–369.
40. Simonelli M. *' Microstructure Evolution and Mechanical Properties of Selective Laser Melted Ti-6Al-4V '*. Loughborough Universityhttp://creativecommons.org/licenses/by-

nc-nd/2.5/ (2014).
41. Bertrand P, Goeuriot P, Smurov I, et al. Ceramic components manufacturing by selective laser sintering. *Appl Surf Sci* 2007; 254: 989–992.
42. Lim S, Prabhu VL, Anand M, et al. Extra-terrestrial construction processes – Advancements, opportunities and challenges. *Adv Sp Res* 2017; 60: 1413–1429.
43. Cooke A, Slotwinski J. Properties of metal powders for additive manufacturing: A review of the state of the art of metal powder property testing. *Addit Manuf Mater Stand Test Appl* 2015; 21–48.
44. Krauss H, Zaeh MFF. Investigations on manufacturability and process reliability of selective laser melting. *Phys Procedia* 2013; 41: 815–822.
45. Wang D, Yang Y, Su X, et al. Study on energy input and its influences on single-track,multi-track, and multi-layer in SLM. *Int J Adv Manuf Technol* 2012; 58: 1189–1199.
46. Meurisse A, Beltzung JC, Kolbe M, et al. Influence of Mineral Composition on Sintering Lunar Regolith. *J Aerosp Eng* 2017; 1–8.
47. Wang D, Yang Y, Liu R, et al. Study on the designing rules and processability of porous structure based on selective laser melting (SLM). *J Mater Process Technol* 2013; 213: 1734–1742.
48. Yadroitsev I, Krakhmalev P, Yadroitsava I, et al. Energy input effect on morphology and microstructure of selective laser melting single track from metallic powder. *J Mater Process Technol* 2013; 213: 606–613.
49. Yadroitsev I, Smurov I. Surface Morphology in Selective Laser Melting of Metal Powders. *Phys Procedia* 2011; 12: 264–270.
50. Bengisu M. *Engineering Ceramics*. Heidelberg, Germany: Springer Science & Business Media, 2001.
51. Olakanmi EO. Selective laser sintering/melting (SLS/SLM) of pure Al, Al-Mg, and Al-Si powders: Effect of processing conditions and powder properties. *J Mater Process Technol* 2013; 213: 1387–1405.
52. Das M, Balla VK, Basu D, et al. Laser processing of SiC-particle-reinforced coating on titanium. *Scr Mater* 2010; 63: 438–441.
53. Kumar S. Selective Laser Sintering/Melting. In: *Comprehensive Materials Processing*. 2014, pp. 93–134.
54. Benaroya H, Bernold L. Engineering of lunar bases. *Acta Astronaut* 2008; 62: 277–299.
55. Lee L-H. Adhesion and cohesion mechanisms of lunar dust on the moon's surface. *J Adhes Sci Technol* 1995; 9: 1103–1124.
56. Sik Lee T, Lee J, Yong Ann K. Manufacture of polymeric concrete on the Moon. *Acta Astronaut* 2015; 114: 60–64.
57. Hoshino BT, Wakabayashi S, Yoshihara S, et al. Key Technology Development for Future Lunar Utilization - Block production using lunar regolith -. 2015; 14: 1–6.
58. DD:ENV:1996-2:2001. Eurocode 6 : Design of masonry structures — Part 2: Design, selection of materials and execution of masonry. *BSI Stand Publ* 2001; 1–70.
59. Vaniman D, Reedy R, Heiken G, et al. The Lunar Environment. In: Heiken G (ed) *Lunar Sourcesbook: A Users Guide to the Moon*. Cambridge University Press, 1991, pp. 27–60.
60. Salisbury JW, Glaser PE, Stein BA, et al. Adhesive behavior of silicate powders in ultrahigh vacuum. *J Geophys Res* 1964; 69: 235–242.
61. Jaumann R, Hiesinger H, Anand M, et al. Geology, geochemistry, and geophysics of

the Moon: Status of current understanding. *Planet Space Sci* 2012; 74: 15–41.